Available online at www.sciencedirect.com
ScienceDirect
Geochimica et Cosmochimica Acta 71 (2007) 3223–3237
Geochimica et Cosmochimica Acta
www.elsevier.com/locate/gca

Mobilization and re-distribution of major and trace elements during extreme weathering of basalt in Hainan Island, South China

Jin-Long Ma [a,b], Gang-Jian Wei [a,*], Yi-Gang Xu [a], Wen-Guo Long [a,c], Wei-Dong Sun [a]

[a] *Key Laboratory of Isotope Geochronology and Geochemistry, Guangzhou Institute of Geochemistry, Chinese Academy of Sciences, Guangzhou 510640, China*
[b] *Graduate School of the Chinese Academy of Sciences, Beijing 100039, China*
[c] *Hainan Bureau of Geology and Mineral Resources, Haikou 570226, China*

Received 22 May 2006; accepted in revised form 28 March 2007; available online 1 May 2007

Abstract

Major, trace and organic elements of a laterite profile developed on Neogene basalts in northern Hainan Island, South China were reported in this paper, the aim of which was to investigate element mobilization and re-distribution during extreme weathering. The results indicate that most of the elements have been mobilized and transferred downwards along the profile by aqueous solution. Organic matter (OM) can significantly improve the transport of insoluble elements. Among all the elements, Th is the least mobile. As for the general conservative elements during incipient chemical weathering, such as Fe, Ti, Zr, Hf, Nb and Ta, the removals are up to 20–40% in the upper profile. However, these elements behave as conservatively as Th in the lower profile. In the middle profile, oxic environment occurs, accompanied with significant OM decomposition. The Mn and Ce transferred downward are readily oxidized into insoluble Mn(IV) and Ce(IV) and precipitate in the oxic front. Important OM decomposition decreases the capacity of transfer of insoluble elements in aqueous solution. Consequently, Al significantly precipitates in the oxic front, and REEs, with the exception of Ce, precipitate largely in the OM-depleted layers. Co and U are also concentrated in the oxic front in association with Mn and Ce, respectively. However, Cr shows a negative correlation with Mn because its response to redox condition changes is reversed from that of Mn. Mn oxides/hydroxides, Fe oxides/hydroxides and secondary phosphate minerals other than clay minerals are potential hosts for REEs except for Ce in the profile; REEs with high concentrations in the profile seem closely associated with Mn oxides/hydroxides. Remarkable, highly correlated, Ce and Gd anomalies are observed in the profile. Ce anomalies are caused by Ce precipitation in the oxic environment and successive decomposition of organic matter. Gd anomalies are likely to have resulted from lower stability constants of Gd–OM complexes compared to those of neighboring REEs. The overall elemental behaviors in this profile suggest that organic matter plays a very important role in the mobilization and re-distribution of the elements during extreme weathering.

1. INTRODUCTION

Chemical weathering of the continent decomposes primary minerals in rocks and activates many elements. As a result, the re-distribution of elements in weathering products is much different from that in parent rocks (Nesbitt, 1979; Nesbitt et al., 1980; Nesbitt and Markovics, 1997).

* Corresponding author. Fax: +86 20 85290130.
E-mail address: gjwei@gig.ac.cn (G.-J. Wei).

0016-7037/$ - see front matter © 2007 Elsevier Ltd. All rights reserved.
doi:10.1016/j.gca.2007.03.035

Weathering products are easily carried out of weathering profiles and deposited in lakes and oceans as the main lithogeneous component in sediments (Windom, 1976). Therefore, the mobilization and re-distribution of elements during chemical weathering may influence the chemical composition of sediments. Generally, sedimental compositions can be used to trace the provenance of sediments (Nesbitt et al., 1996) and to reconstruct paleoclimate records (Zabel et al., 2001; Wei et al., 2004). Comprehensive understanding of the behavior of elements during chemical weathering may help to better explain the records found in sediments.

Chemical weathering has been investigated for a long time (Craig and Loughnan, 1964; Harriss and Adams, 1966), and the behaviors of elements have been well classified. In general, alkalis and alkaline earth elements are easily removed from primary minerals during chemical weathering (Nesbitt et al., 1980; Chesworth et al., 1981; Nesbitt and Wilson, 1992; Nesbitt and Markovics, 1997). On the contrary, elements that are predominantly hosted in highly resistant minerals, such as Zr and Hf in granitic rocks, are believed to be immobile (Nesbitt and Markovics, 1997). Some other elements, such as Al, Fe and Ti tend to be combined with secondary minerals and to be retained in the soil profile during chemical weathering (Chesworth et al., 1981; Nesbitt and Wilson, 1992; Nesbitt and Markovics, 1997). Of all the elements, much attention has been paid to the rare earth elements (REEs) in the past several decades (Nesbitt, 1979; Duddy, 1980; Banfield and Eggleton, 1989; Marsh, 1991; Price et al., 1991; Caggianelli et al., 1992; Nesbitt and Wilson, 1992; Braun et al., 1993, 1998; Mongelli, 1993, 1997; Boulange and Colin, 1994; Condie et al., 1995; Koppi et al., 1996; Nesbitt and Markovics, 1997; Hill et al., 2000; Patino et al., 2003). Despite some discrepancies between different studies, there is a consensus that REEs are mobile during chemical weathering, and re-distribution of REEs in weathering products varies with weathering intensity.

Most of the studies mentioned above, however, were carried out in temperate zones with weathering intensities from incipient to advanced degree. The behavior of elements during extreme weathering has been far less studied. Studies in tropical regions indicate that the mobilization and re-distribution of elements during chemical weathering are different from those of temperate zones (Braun et al., 1993, 1998; Young and Nesbitt, 1998; Hill et al., 2000; Kurtz et al., 2000; Dequincey et al., 2002). Elements that are conserved in temperate zone, such as Ti and Zr, are mobile during extreme chemical weathering in tropical regions (Braun et al., 1993, 2005; Melfi et al., 1996; Nahon and Merino, 1996; Cornu et al., 1999), and dissolved organic matters can significantly improve the transfer of insoluble elements, such as Al, Fe, Zr, Ti and Th (Viers et al., 1997, 2000; Oliva et al., 1999; Braun et al., 2005). Because extreme weathering is the highest stage of the weathering process, probing into element behavior during this particular period is pivotal to understanding element mobilization and re-distribution during chemical weathering. Furthermore, laterites, the products of extreme weathering, account for over 85% of the present world soil cover (Nahon, 2003). They are readily eroded from profiles and transported into oceans, and their chemical compositions may be imprinted into sediments. Thus, understanding the behavior of elements during extreme weathering may aid in our understanding of the chemical record in sediments and soils.

Herein, we report some major and trace elements of a weathering profile developed on Neogene basalt in northeast Hainan Island, South China. Because basalts are very sensitive to chemical weathering (Berner and Berner, 1997), and chemical weathering is significantly intensified by the tropical climate, most of the weathering profiles in this region have undergone extensive weathering. In this paper, we compare the composition of weathering products with fresh parent rocks to investigate element mobilization and re-distribution during the processes of advanced to extreme weathering.

2. GEOLOGICAL SETTING, WEATHERING PROFILE AND SAMPLING

Numerous lateritic weathering profiles have developed on the basalts, which erupted during the Neogene and Quaternary in the northern Hainan Island, South China (Huang et al., 1993). The basaltic weathering profile under study is located in Wenchang County, about 60 km south of Haikou, the capital city of Hainan Province. Climate in this region is tropical style, controlled by the East Asian monsoon. The mean annual temperature is about 25 °C, with the maximum monthly temperature, 30–32 °C, occurring during July to August, and the minimum monthly temperature, 18–20 °C, occurring during January and February. Annual precipitation varies from 800 to 2500 mm (during the past century), with an average of about 1500 mm. Over 80% of precipitation occurs in the warm season, from May to October.

The profile, located on a small hill (19°34′74″N, 110°38′71″E), has been recently cut by a stone quarry. The slope of the hillside is gentle, and the depth of the weathering profile ranges from over 6 m above the fresh basalt at the hill center to about 3 m at the edge of the hill. The sampling profile was selected in the middle of the hillside, which is newly cut (less than 1 month) and has a flat top. Interruption is not observed in the intergradation from basalt to laterite; thus, we expected that this profile developed continuously since the eruption of the basalt. Fig. 1 shows the details of the sampling profile. The top 30 cm is loose soil, covered with flourishing plants. Pepper has been planted in this region for at least one year; therefore, the top soil may have been disturbed during farming. Beneath, there is a laterite layer about 20 cm thick containing gravels. The gravels are well abraded and have an oval shape with sizes ranging primarily from 2 to 5 cm. Not all the gravels are basalts. This indicates that the top soil and the gravel layer may not have entirely developed from the basalt beneath. In order to avoid influence from different sources, we did not collect samples in these sections. Beneath the gravel layer, there is no sign of disturbance in the saprolite profile and the laterites are in-situ weathering products developed from the basalts (Fig. 1). Samples

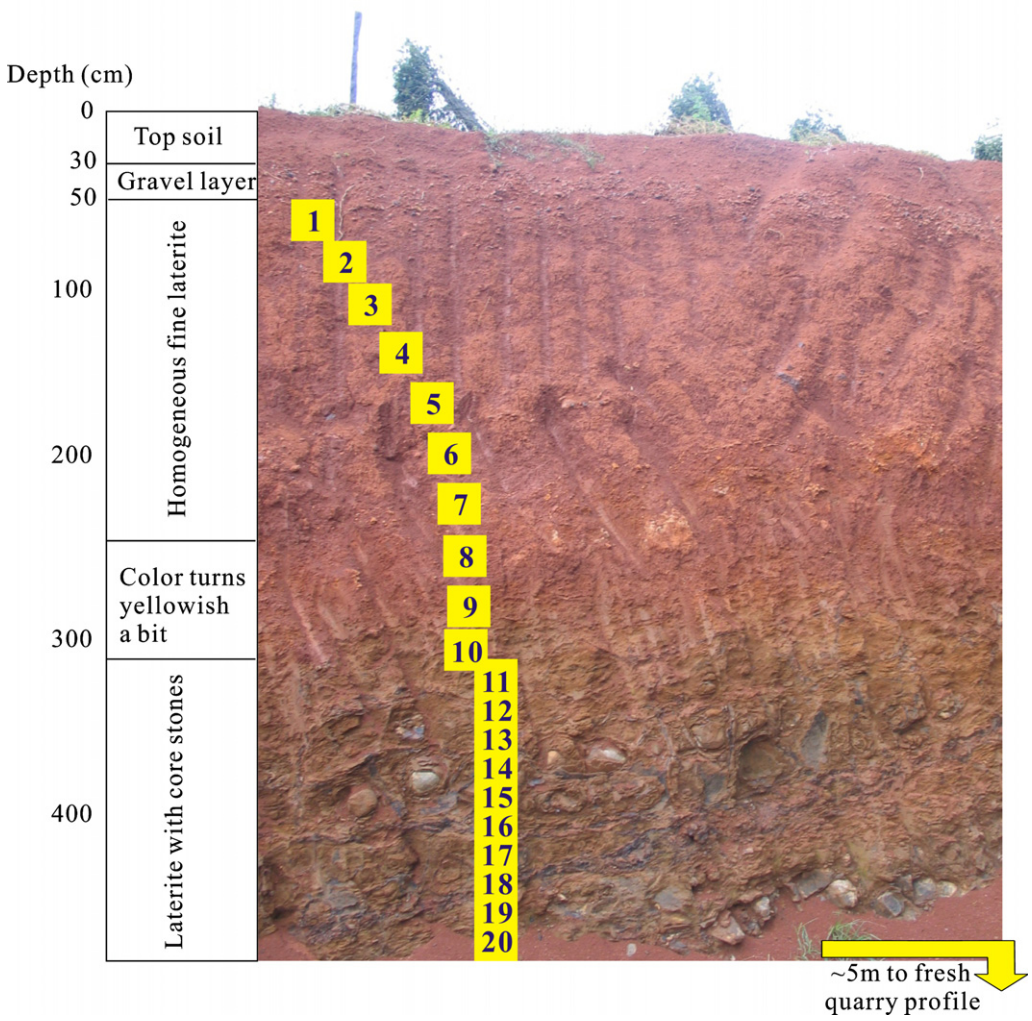

Fig. 1. Outlook of the profile. The image shows the sampling profile, and numbers indicate the sample ID and their sampling position in the profile.

were taken downward in the profile. The upper 250 cm is fine laterite in a homogeneous red color, and the sampling interval is about 30 cm (HK06-1 to HK06-7). The soil between 250 and 320 cm is still fine in grain size. The soil color turns a little yellowish, but basically remains red. Several samples (HK06-8 to HK06-10) were collected in this section. The soil color becomes pistachio below 320 cm with un-weathered core stones, and black shell-shaped matter fills the area between the core stones. Both the soil and the black shell-shaped material were sampled together in an interval of 10–15 cm (HK06-11 to HK06-20).

The quarry profile, where the two parent rock samples (HK06-R1 and HK06-R2) were collected, is next to the sampling profile. The distance between the two basalt samples is over 30 m. The parent rock is fresh tholeiitic basalt. The main phenocryst is pyroxene (10%), which is only slightly chloritized. The groundmass consists of plagioclase (60%), clinopyroxene (25%) and opaque minerals, mainly ilmenite (5%). No other accessory minerals could be identified in the slices. The age of the basalts in this region is ~4.0 Ma dated by K–Ar chronology (Zhu and Wang, 1989).

3. ANALYTICAL METHODS

The laterite samples were first dried at ~70 °C, and then both the dried laterites and the fresh basalts were ground into powder. The powder was baked at 105 °C to remove absorbed water before analysis. Major elements were measured using a Rigaku ZSX100e X-ray fluorescence (XRF) on glass discs, made by fusing 0.5000 g sample powder and 4.0000 g $Li_2B_4O_7$ at 1200 °C. Analytical precision for major elements is better than 1%, and determination limits for the major elements are generally better than 30 ppm. The sample powder was first baked at 700 °C to destroy organic matters, and then digested by mixed acid solution of $HNO_3 + HF$ for trace element measurement. Trace elements were measured using a Perkin-Elmer Elan 6000 ICP-MS with detection limits of about several pg/g in solution, corresponding to a determination limit of about 10 ppb in solid samples for trace elements. Analytical precision for trace elements is better than 5% (Liu et al., 1996). For the weathering product samples, most of the CaO, Na_2O and K_2O are close to the determination limits of

Table 1
Major element (in %) and trace element (in ppm) concentrations of the samples in basaltic weathering profile

	HK06-1	HK06-2	HK06-3	HK06-4	HK06-5	HK06-6	HK06-7	HK06-8	HK06-9	HK06-10	HK06-12	HK06-13	HK06-14	HK06-15	HK06-16	HK06-17	HK06-18	HK06-19	HK06-20	HK06-R1	HK06-R2
Depth(m)	0.50	0.90	1.30	1.60	1.90	2.20	2.50	2.80	3.00	3.20	3.50	3.65	3.80	3.95	4.10	4.20	4.30	4.40	4.50	—	—
SiO_2	31.23	31.49	31.82	29.38	26.38	28.38	27.99	25.98	25.28	19.71	34.01	34.03	26.20	30.73	20.80	19.66	24.37	27.65	17.49	51.77	52.00
TiO_2	5.17	4.67	4.09	4.08	4.47	4.27	3.98	3.70	2.71	4.72	3.56	2.95	4.08	3.61	5.01	4.91	5.30	4.61	5.29	1.85	1.91
Al_2O_3	26.71	27.20	27.88	30.46	28.31	28.51	29.84	32.18	36.16	30.26	26.84	30.05	28.69	28.06	28.05	28.09	26.73	25.82	31.60	14.12	14.25
Fe_2O_3T	23.48	23.45	22.69	21.62	24.40	23.41	20.97	20.43	15.74	25.52	19.32	15.23	23.40	19.44	27.23	27.62	27.65	23.74	27.04	10.33	10.56
MgO	0.27	0.25	0.23	0.21	0.26	0.33	0.40	0.57	0.49	0.60	0.84	0.81	0.64	0.87	0.63	0.68	0.76	0.50	0.50	7.26	7.41
MnO	0.09	0.09	0.09	0.09	0.12	0.15	0.25	0.41	0.250	0.16	0.61	0.62	0.24	0.20	0.23	0.15	0.13	0.38	0.16	0.13	0.14
$CaO^{\#}$	0.02	0.02	0.02	0.02	0.02	0.02	0.02	0.01	0.01	0.01	0.01	0.00	0.00	0.00	0.00	0.01	0.01	0.01	0.00	8.82	8.93
$Na_2O^{\#}$	0.04	0.13	0.11	0.03	0.06	0.03	0.04	0.05	0.05	0.03	0.12	0.02	0.10	0.02	0.02	0.05	0.01	0.09	0.04	2.56	2.65
P2O5	0.17	0.8	0.17	0.18	0.22	0.23	0.28	0.31	0.34	0.66	0.41	0.27	0.55	0.46	0.81	0.81	0.69	0.47	0.77	0.28	0.31
$K_2O^{\#}$	0.17	0.15	0.10	0.08	0.06	0.05	0.07	0.02	0.02	0.02	0.04	0.04	0.04	0.04	0.05	0.05	0.05	0.03	0.01	0.70	0.77
LOI	12.63	12.98	13.06	17.14	15.55	15.07	15.91	16.91	18.71	18.61	14.65	15.84	16.19	16.46	17.53	18.44	14.23	17.14	17.26	1.63	1.51
Total	99.99	100.60	100.26	100.49	99.85	100.44	99.75	100.57	100.50	100.28	100.40	99.87	100.16	99.89	100.37	100.47	99.93	100.44	100.17	99.46	100.42
TOC	0.15	0.14	0.15	0.13	0.13	0.11	0.10	0.07	0.07	0.08	0.04	0.06	0.08	0.08	0.150	0.06	0.12	0.14	0.11	—	—
TN	0.017	0.016	0.032	0.004	0.008	0.026	<DL	<DL	<DL	<DL	<DL	<DL	0.006	<DL	<DL	0.006	<DL	0.022	0.029	—	—
pH	5.18	5.16	5.30	5.26	5.38	5.33	5.09	5.14	5.53	5.52	5.64	5.70	5.43	5.74	5.76	5.72	5.78	5.42	5.70	—	—
Sc	35.9	37.4	35.1	33.9	41.2	41.2	41.2	40.3	37.2	44.2	34.6	28.2	46.8	36.7	55.5	41.8	49.6	41.1	50.1	19.5	17.9
V	291	302	284	281	337	358	347	349	248	315	260	193	288	248	352	317	372	320	346	141	136
Cr	447	427	361	534	441	332	369	359	319	6261	326	107	675	410	834	677	783	331	752	231	208
Mn	569	555	585	569	871	1116	1887	3092	7745	1074	4923	5268	16	1538	1697	981	928	3133	1097	1068	963
Co	30.2	17.9	42.8	24.6	259	354	161	243	803	80.1	205	234	82.0	77.8	57.9	91.7	44.6	154	61.1	106	95.3
Ni	172	179	179	174	210	246	304	3118	395	436	496	569	459	472	402	606	352	393	270	159	149
Cu	118	120	119	124	146	158	160	144	173	237	229	163	237	185	236	362	234	239	233	71.3	67.0
Zn	105	102	94.3	96.9	110	116	108	92.3	93.2	153	135	102	124	114	129	187	134	110	125	99.2	96.4
Ga	40.7	41.6	39.7	39.5	43.7	41.6	39.2	37.8	35.5	44.8	34.3	28.5	39.4	33.7	46.1	45.5	47.2	41.4	48.4	19.1	17.6
Ge	2.22	2.28	2.20	2.18	2.23	2.71	2.52	3.442	2.60	2.55	2.98	3.75	3.88	3.47	3.44	2.67	3.30	2.93	2.43	1.30	1.17
Rb	9.57	7.82	5.32	4.25	3.79	3.89	3.06	1.88	1.76	2.27	4.33	3.20	3.76	4.45	5.97	5.28	5.84	2.89	1.65	16.8	15.4
Sr	25.52	25.44	21.54	18.97	13.35	10.40	7.71	3.96	4.25	2.39	3.20	1.84	1.24	1.43	1.36	2.57	2.99	5.22	2.43	286	275
Y	14.0	12.8	11.3	10.01	10.8	10.5	12.9	14.8	20.3	30.0	114.8	18.3	23.6	27.9	24.7	51.8	55.9	62.5	51.2	20.9	20.1
Zr	302	300	274	285	281	267	267	213	163	278	207	176	236	210	285	271	299	297	297	126	119
Nb	61.1	57.8	49.7	50.2	51.2	49.0	42.0	39.5	29.2	51.2	38.2	32.6	4.62	38.5	52.4	50.3	55.3	53.0	54.6	21.5	22.6
Cs	1.71	1.51	1.09	0.85	0.76	0.69	0.45	0.41	0.35	0.31	0.44	0.35	0.35	0.38	0.4	0.46	0.54	0.42	0.28	0.36	0.31
Ba	62.0	57.7	48.7	43.0	43.8	43.9	48.1	44.6	72.1	155	251	198	138	151	119	222	108	2430	117	236	196
La	40.3	39.0	36.2	32.0	23.1	21.6	20.5	22.0	23.1	29.6	104	26.8	3.1	41.4	34.2	65.0	77.2	84.2	63.1	15.9	16.6
Ce	67.1	73.0	101	81.1	106	162	203	352	1107	123	159	243	104	130	87.2	72.6	169	323	154	30.3	30.7
Pr	7.41	7.45	7.00	6.13	4.58	4.83	5.22	6.89	7.16	10.1	33.7	8.88	11.3	14.4	12.2	23.4	27.1	28.5	21.6	3.80	3.73
Nd	27.5	26.7	25.2	22.0	17.7	20.2	23.9	33.5	34.1	51.1	170	44.1	59.2	71.6	62.2	121	137	147	111	17.5	17.2
Sm	4.95	4.85	4.51	4.11	3.62	4.41	5.50	8.29	8.57	12.6	41.0	9.87	13.5	16.1	14.6	26.9	31.2	32.4	26.0	4.56	4.44
Eu	1.34	1.31	1.23	1.12	1.05	1.27	1.56	2.39	2.51	3.55	11.8	2.57	3.50	4.13	3.89	6.94	8.06	8.36	7.03	1.51	1.48
Gd	3.86	3.70	3.70	3.20	3.08	4.08	5.36	8.36	13.5	10.4	37.7	8.21	9.47	19	10.9	18.8	22.3	24.9	19.7	4.88	4.91

Tb	0.57	0.54	0.50	0.46	0.46	0.56	0.73	1.09	1.29	1.55	5.53	1.09	1.48	1.62	1.56	2.61	3.19	3.39	2.88	0.80	0.75
Dy	2.97	2.81	2.64	2.34	2.44	2.95	3.76	5.66	6.01	8.23	28.3	5.42	7.58	8.52	8.29	13.8	16.5	17.7	15.1	4.28	4.12
Ho	0.52	0.50	0.45	0.41	0.41	0.50	0.64	0.96	1.05	1.42	5.07	0.95	1.30	1.43	1.37	2.44	2.85	3.05	2.57	0.81	0.79
Er	1.49	1.36	1.21	1.17	1.11	1.38	1.75	2.58	2.83	3.90	13.8	2.67	3.57	4.14	3.83	6.86	8.07	8.84	7.28	2.07	1.99
Tm	0.19	0.18	0.16	0.15	0.15	0.19	0.24	0.36	0.39	0.53	180	0.37	0.49	0.56	0.53	0.92	1.13	1.22	1.01	0.26	0.25
Yb	1.33	1.20	1.13	1.05	1.04	1.33	1.60	2.36	2.55	3.39	10.7	2.44	3.30	3.74	3.54	5.79	7.03	7.57	6.50	1.59	1.53
Lu	0.20	0.19	0.17	0.15	0.15	0.18	0.23	0.33	0.35	0.49	1.54	0.35	0.47	0.52	0.48	0.83	0.99	1.09	0.92	0.24	0.22
Hf	14.7	14.2	13.6	13.5	14.7	14.3	12.0	10.9	7.98	14.4	10.8	8.78	12.4	11.0	15.5	14.9	16.7	15.7	16.4	5.36	5.02
Ta	3.95	3.60	3.31	3.20	3.43	3.33	2.79	2.56	1.93	3.32	2.54	2.13	2.93	2.57	3.43	3.31	3.79	3.65	3.66	1.32	1.37
Pb	12.5	12.3	12.1	10.7	14.3	12.6	9.57	5.82	4.90	5.21	5.67	6.37	6.08	6.07	6.50	5.93	5.39	8.91	6.02	3.41	3.52
Th	9.20	9.19	8.58	7.90	7.83	7.10	5.86	5.02	3.72	5.99	4.90	3.87	5.21	4.74	6.37	5.97	6.81	6.70	6.58	2.46	2.63
U	1.96	1.95	1.78	1.69	1.89	1.58	1.52	1.74	1.87	1.25	1.03	0.71	1.19	0.87	1.54	1.14	1.50	1.31	2.03	0.55	0.60
Ce/Ce^*	0.99	1.09	1.61	1.48	2.63	4.07	5.03	7.26	21.89	1.79	0.68	3.99	1.37	1.34	1.07	0.47	0.93	1.67	1.05	—	—
Gd/Gd^*	0.95	0.94	1.02	0.96	0.97	1.06	1.09	1.13	1.63	0.96	1.02	1.03	0.87	0.89	0.87	0.93	0.93	0.98	0.94	—	—

[#]Data measured by ICP-AES; Fe_2O_3T: total Fe.

<DL, less than detection limit; —, no measurement or no calculation.

$Ce/Ce^* = 2(Ce/Ce_P)/(La/La_P + Pr/Pr_P)$; $Gd/Gd^* = 3(Gd/Gd_P)/(Sm/Sm_P + 2Tb/Tb_P)$: where P indicates normalized to the parent rock, which are averaged from the two fresh basalts.

Table 2
Mineralogy of the weathering products from the profile

	HK06-1	HK06-2	HK06-3	HK06-4	HK06-5	HK06-6	HK06-7	HK06-8	HK06-9	HK06-10	HK06-12	HK06-13	HK06-14	HK06-15	HK06-16	HK06-17	HK06-18	HK06-19	HK06-20
Kaolinite	82	73.1	79.3	73.9	43.8	64		62	28.3										20
Halloysite							53.4			30.7	82.6	87.4	60.3	63.5	38.8	39.2	35.4	59.8	
Illite							16.3												
Gibbsite				13.7	21	11.4	18.7	25.5	53	48.5		7.6	25.3	24.6	45.1	48	32.6	18.5	60
Ilmenite	5.4		7.6	3	7.8	9.6		5.2	3.5	7.4	4.2		9.4	8.9	7.3	8.5		6.7	
Goethite	8	10.6	5.5		7.6	5.1	5.1	4.2	4.2		5.2				5.8			4.5	
Magnetite		6.2								8.2	4						14.9	7.5	
Hematite		6.3	4.6	6.4			3.4										14.1		12
Amorphous Phase and others	4.6	3.8	3	3	19.8	3.1	3.1	3.1	11	5.2	4	5	5	3	3	4.3	3	3	8

XRF. These elements were measured on a Varian Vista Pro ICP-AES with detection limits of several ng/g in solution, corresponding to several ppm determination limits in solid samples. The solutions for ICP-MS measurement were used for these tests. Analytical details are described in Li et al. (2002), and precision for these elements is better than 1%. The CaO, Na_2O and K_2O of the two fresh basalt samples were also double-checked by ICP-AES, and the results agreed with those obtained by XRF. Both major and trace element analyses were carried out in the Key Laboratory of Geochronology and Geochemistry, Chinese Academy of Sciences. The analytical results are presented in Table 1. Several USGS and Chinese soil and basalt standard references, such as GSS-5, GSS-7, GXR-6 (soils) and BHVO-2, BCR-2 (basalt) were repeatedly measured with the samples to monitor the quality of ICP-MS and ICP-AES measurements, and the results were generally within the range of ±10% of the certified values.

Total organic carbon (TOC) and total nitrogen (TN) contents of the weathering profile were determined using a Vario EL III elemental analyzer with detection limits of about 30 μg for C and N. Samples were passed through a 100-mesh sieve to remove possible plant roots, which could be seen in samples taken from the top 1 m of the profile. The combustion temperature was set at 960 °C. About 10–30 g of sample was used for a single measurement. Duplicates of every sample were analyzed, and reproducibility of the two measurements was better than 5% for TOC and TN. The average of the two measurements was adopted for TOC and TN concentrations, and the results are also listed in Table 1.

The pH values of the weathering products were also measured. Ten gram of de-ionized water was first equilibrated with 5 g sample powder in a capped Teflon beaker for 8 h, and then the liquid was collected by filtration. The pH values of the liquid were measured using an Orion $210A^+$ acidity meter with precision better than 0.05. The results are also listed in Table 1.

Mineral compositions of the samples were measured on a Rigaku D/max-1200 diffractometer in the Guangzhou Institute of Geochemistry, CAS. X-ray diffraction (XRD) patterns of the samples were recorded between 1.5° and 20° (2θ) at a scanning speed of 2°/min with Cu Kα radiation (30 mA and 40 kV). The results are listed in Table 2.

4. RESULTS

Kaolin-group minerals, oxides and hydroxides dominate in the weathering products. Kaolin and halloysite contents are from 20% to 87%, gibbsite abundance ranges from 0% to 60%, and ilmenite, goethite, magnetite and hematite account for 7–29%. Secondary minerals, such as smectites and illites, are absent except in sample HK06-7, which contains about 16% illites.

Some of the major elements, such as TiO_2 (2.71–5.30%), Al_2O_3 (25.82–36.16%) and Fe_2O_3(T) (15.23–27.65%) are markedly enriched in the weathering products, which are about 2- to 3-fold higher than in the fresh basalt. Concentrations of MnO and P_2O_5 in the top 2.5 m of the profile are slightly lower than those in the fresh basalt, but they increase in the lower section. SiO_2 concentrations in weathering products range from 17.49% to 34.03%, compared with ~52% in the fresh basalts. Concentrations of MgO (0.21–0.87%), CaO (<0.05%), and Na_2O and K_2O (<0.1%) are dramatically lower than in the fresh basalt. Loss of ignition (LOI) accounts for 12.6–18.7% of the weathering products, and LOI in the lower section is generally higher than in the upper section.

Elements in the weathering products, except for Rb, Sr and Ba, are higher than in the fresh basalts. Most trace elements show higher concentrations in the lower profile than in the upper profile, whereas U, Th, Cs, Rb and Sr show higher concentrations in the top 2.5 m of the profile.

TOC and TN concentrations vary from 0.04% to 0.15% and from 0% to 0.03%, respectively. In the middle profile (2–4 m), concentrations of TOC and TN become lower, and TN is even under detection limit.

Concentrations of major and trace elements in the two fresh basalts are very similar (Table 1). In particular, the concentrations of Ti, Zr, Hf, Nb, Ta and Th are the same within analytical errors. As the sampling distance of the two fresh basalts is over 30 m, the similarity suggests that the elemental distribution in the fresh basalt is homogeneous, at least at the scale of the sampling profile.

5. DISCUSSION: MOBILIZATION AND RE-DISTRIBUTION OF ELEMENTS

Several indexes, such as chemical index of alteration (CIA), weathering index (WI) and intensity of chemical weathering (CIW) have been proposed to evaluate the intensity of chemical weathering (Parker, 1970; Nesbitt, 1979; Harnois, 1988). Because they are all calculated from concentrations of mobile elements, such as CaO, Na_2O and K_2O, these indexes are only suitable for incipient to intermediate weathering, and inappropriate for intensive chemical weathering (Nesbitt and Wilson, 1992; Patino et al., 2005).

Concentrations of CaO, Na_2O, MgO and K_2O in the weathering products are extremely low compared to the fresh basalt (Table 1). They are even significantly lower than those in the advanced zone reported by Nesbitt and Wilson (1992). As a result, CIA values in this profile are greater than 99%. On the contrary, concentrations of Al_2O_3, Fe_2O_3(T) and TiO_2 are very high, with maximum values up to 36%, 27% and 5.3%, respectively. This suggests that the chemical weathering intensity in this profile could be categorized as extreme (Nesbitt and Wilson, 1992).

Mass balance calculation is one of the best methods used to investigate the mobilization of elements during chemical weathering, in particular, to estimate the fluxes for elements to be added into or removed from the profile (Brimhall et al., 1991). If no volume change between weathering product and parent rock is assumed (Nahon and Merino, 1996), mobilization of an element can be described as percentage changes of elemental ratios to a conservative element relative to parent rock (Nesbitt, 1979) as following:

$$\%\ \text{change of ratios} = 100 \times [(R_i - R_p)/R_p]$$

where R_i and R_p represent the ratio of element to a conservative element in weathered samples and fresh basalt,

respectively. The conservative element selected for evaluating element mobilization may vary in different profiles. K has been used to evaluate the mobility of alkali and alkali earth elements during incipient weathering processes (Nesbitt et al., 1980), and Zr is used in granitic weathering profiles (Nesbitt and Markovics, 1997). In basaltic weathering profiles, Ti is generally used as the conservative element (Nesbitt and Wilson, 1992; Hill et al., 2000). However, other studies indicate that Th is the least mobile element compared to Zr and Ti during lateritic weathering (Braun et al., 1993). According to Nesbitt and Wilson (1992), the order for element to be leached from basalt is not fixed, and is controlled by the mineralogical site of the concerned elements in the parent basalt. Therefore, selection of conservative elements may vary in different profiles.

5.1. Conservative elements

Ti, Fe, Zr, Hf, Nb, Ta and Th are potential conservative elements in basaltic weathering profiles because they are generally hosted in resistant minerals (Nesbitt and Wilson, 1992; Braun et al., 1993; Hill et al., 2000; Kurtz et al., 2000). However, resistant heavy minerals, such as zircon, are not identified in the cryptocrystalline groundmass of the fresh basalt and in the weathering products. Thus, it is difficult to determine the least mobile elements by mineral compositions. One way to sort the conservation sequence of these elements is to compare the percentage changes of their ratios to one particular element, relative to the fresh basalt. This may provide information for the relative mobility of these elements during extreme weathering. Following Braun et al. (1993), Th is assumed to be the most immobile element, and the percentage changes of Ti, Fe, Zr, Hf, Nb and Ta to Th ratios relative to the fresh basalt are calculated and shown in Fig. 2.

The percentage changes of Ti, Fe, Zr, Hf, Nb and Ta to Th ratios relative to the fresh basalt are all negative in the upper 3.0 m of this profile, with minimum values occurring in the top section (0.5–1.3 m) (Fig. 2). The minimum values for Fe/Th and Zr/Th are about −40%, about −35% for Ti/Th and Nb/Th, and about −30% for Hf/Th and Ta/Th. This confirms the assumption that Th is the most immobile of these elements in the upper profile. Assuming Th is conservative, about 30–40% of Ti, Fe, Zr, Hf, Nb and Ta may have been removed from the top section of the profile, indicating that these elements are quite mobile during extreme weathering.

The percentage changes of these ratios gradually become less negative downwards in the profile, and remain nearly constant in the section below 3 m. The averages for Zr/Th and Nb/Th in this section are about −13% and −6%, respectively, suggesting a slight loss of Zr and Nb in the lower profile, whereas the average for Hf/Th is about 8%, implying some gain of Hf in the lower profile. However, the average percentage changes of Fe/Th, Ti/Th and Ta/Th below 3 m are within the range of ±2% relative to the fresh basalt, suggesting that they are as conservative as Th in the lower section of the profile.

Such variation patterns suggest that Fe, Ti, Zr, Hf, Nb and Ta are all mobile during extreme weathering compared to Th. They are gradually removed from the upper section of the profile and transferred downwards. Only a small part of Hf seems to be retained in the lower profile. Most of these elements, however, are carried away from the profile.

The mobilization of these elements may be accounted for by the relatively stronger acid environment and higher organic matter in the upper profile. The pH values of the weathering products are all less than 5.8 and they are less than 5.5 in the section above 3 m (Fig. 2). The pH values increase consecutively, while TOC contents decrease

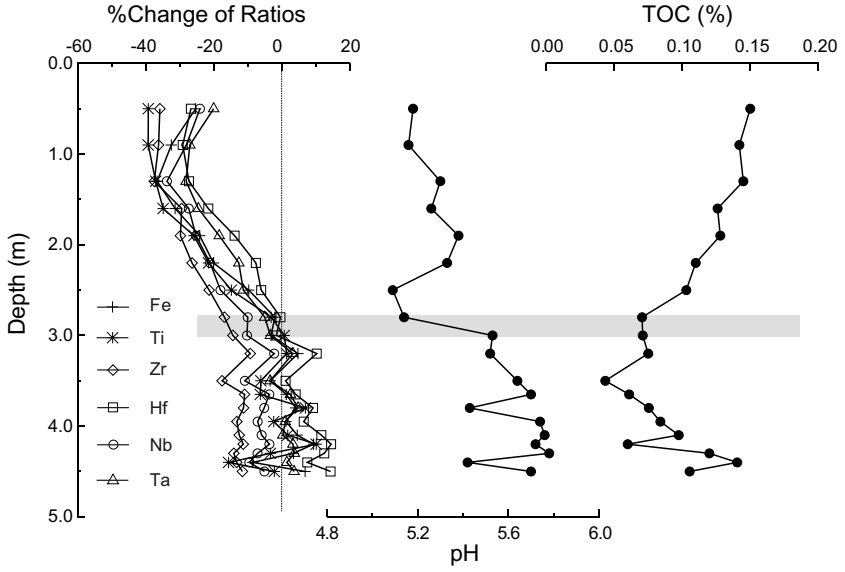

Fig. 2. In-depth variations of the percentage changes of Fe, Ti, Zr, Hf, Nb and Ta to Th ratios relative to the fresh basalt, pH values as well as TOC concentrations. The shaded bars indicate the layer in which percentage change of these ratios turn to constant.

successively downwards in the profile in the top 3 m, accompanied by increasing percentage changes of Fe, Ti, Zr, Hf, Nb and Ta to Th ratios relative to the fresh basalt (Fig. 2). The acid environment favors the decomposition of the primary minerals in which these elements are hosted, and organic matter may form organic colloids that can significantly improve the transport of insoluble elements such as Ti, Zr, and Th in aqueous solution (Viers et al., 1997; Dupre et al., 1999; Oliva et al., 1999; Braun et al., 2005). Therefore, these elements, which seem to be transferred by organic matter, are depleted in the upper profile. In principle, Th may also be mobilized in such an acid environment and removed from the profile with organic matter. However, Th appears to be more resistant to such an environment, compared to other elements.

5.2. Al, Mn, Co, Ce, U and Cr

The percentage changes of Al/Th, Mn/Th, Co/Th and Ce/Th ratios relative to the fresh basalt in the top section (0.1–1.0 m) are about −50%, −80%, −95% and −40%, respectively (Fig. 3), indicating significant removal of Al, Mn, Co and Ce. On the contrary, U is almost completely conserved in the top 2.0 m with percentage change of U/Th ratios relative to the fresh basalt ranging from −7.0% to 8.0% (Fig. 3). Losses of Al, Mn, Co and Ce decrease successively downwards in the profile. The percentage changes of Al/Th, Mn/Th and Co/Th relative to the fresh basalt become positive at 2.5–2.8 m, and those of Ce/Th and U/Th at about 1.9 m, indicating significant enrichment of these elements in the middle profile (2.8–3.7 m) with a maximum occurring at about 3 m (Fig. 3). The most prominent enrichment is presented by Ce, with percentage changes of Ce/Th ratios up to 2300% relative to the fresh basalt. The maxima of Mn/Th and Co/Th are about 400%, and about 120% and 70% for U/Th and Al/Th, respectively. Such a pattern indicates that Al, Mn, Co, Ce and U are removed from the upper profile, transferred downwards, and then precipitated in the middle profile, resulting in remarkable enrichment compared to the fresh basalt.

Mn is liable to be leached from primary minerals during chemical weathering of basalt (Nesbitt and Wilson, 1992). Generally, Mn(II) is soluble and thus can be easily transferred by aqueous solutions. However, when it is oxidized into Mn(IV), Mn precipitates as insoluble oxides or hydroxides in the weathering profile (Koppi et al., 1996). Likewise, Ce(III) is soluble in a reduced environment, but Ce become insoluble when oxidized to CeO_2 in oxic environments (Braun et al., 1990).

Given that Mn and Ce exhibit the same distribution pattern, it is highly possible that a change in redox condition is the key to controlling the mobilization and distribution of Mn and Ce in the profile. Supposing that the weathering profile resembles the sediment columns, where organic matter is the most important reductant as a result of its decomposition by oxygen (Froelich et al., 1979), changes of the redox condition in the weathering profile may be closely associated with organic matter. TOC contents are also plotted in Fig. 3. The successive downward decrease of TOC content in the upper 3.0 m suggests that the redox condition gradually turns from anoxic in the upper profile to oxic in the middle profile. This is further supported by variations in the organic nitrogen concentration. Organic nitrogen is stable in a reduced environment, but easily oxidized to nitrate in oxic environments (Froelich et al., 1979). Because the highly soluble nitrate can not precipitate in the weathering profile, TN mainly represents organic nitrogen. TN is detectable in the upper 3 m section but absent in the middle profile (Fig. 3), indicating an oxic environment in the middle profile and a reduced environment in the upper profile. Such a redox condition pattern agrees well with the successive removal of Mn and Ce in the upper profile and the enrichment in the middle profile.

The distribution of Co is very similar to that of Mn and Ce, and concentrations of Co and Mn are highly correlated, with a correlation coefficient of about 0.80. This suggests that Co distribution is sensitive to change of redox condition in this profile.

Because the oxic phases of U, such as UO_2^{2+}, are very soluble, oxic environment alone may not result in U enrich-

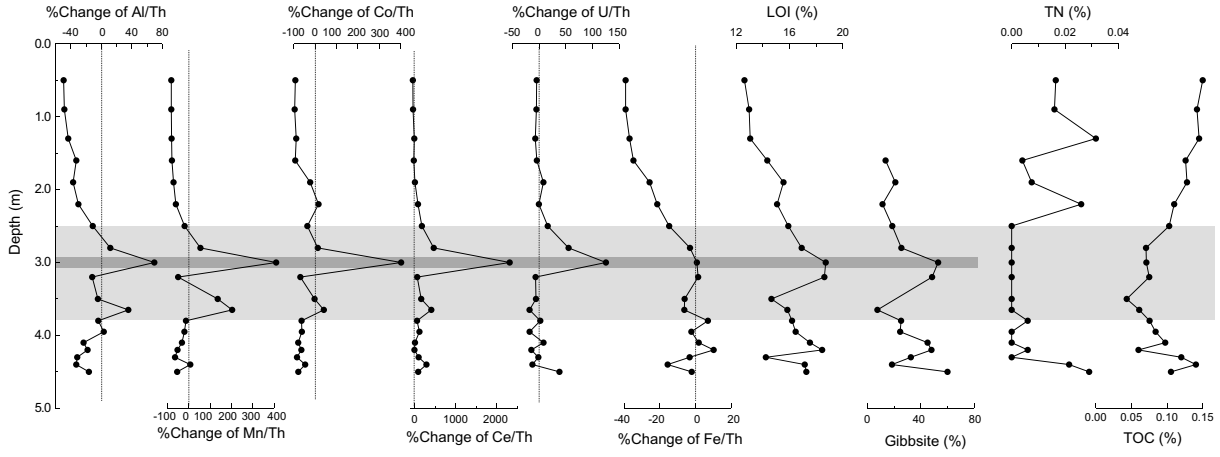

Fig. 3. In-depth variations of the percentage changes of Al/Th, Mn/Th, Co/Th, Ce/Th and U/Th ratios relative to the fresh basalts and LOI, gibbsite contents, TOC and TN concentrations. The shaded bar shows the range of oxic environment, and the darker bar shows the oxic front. The vertical dashed lines indicate a value of zero.

ment. Some studies suggest that CeO_2 may act as nucleating sites and result in U precipitation in weathering profiles (Koppi et al., 1996). Therefore, the U enrichment in the middle profile could be associated with Ce enrichment.

Distribution of Al in this profile cannot be related to redox condition change because Al has no variable valence. Al is basically insoluble in the weathering profile and is difficult to transfer by aqueous solution (Nesbitt and Wilson, 1992). However, in tropical environments, organic colloids formed from OM degradation can significantly improve Al mobilization (Dupre et al., 1999; Oliva et al., 1999; Viers et al., 2000; Braun et al., 2005). The variation of TOC contents agree well with the distribution of Al. A successive downward decrease of TOC content in the upper profile suggests that Al is gradually removed from the upper profile and transferred downward, in association with organic colloids. In the middle profile, where the oxic environment prevails, large amounts of organic colloids are decomposed, and the capacity to carry Al declines significantly, resulting in precipitation of Al.

In addition to organic colloids, Fe-colloids can significantly concentrate some of the trace elements, and improve their transferring ability during weathering (Pokrovsky et al., 2006). Thus, precipitation of Fe oxide/hydroxide may also result in element enrichments in the weathering profile. The percentage change of Fe/Th is also shown in Fig. 3. Unlike those for Al, Mn, Co, Ce and U, no significant enrichment of Fe is observed in the middle profile relative to the fresh basalt. This indicates that the contribution of Fe-colloids to the enrichment of Al, Mn, Co, Ce and U is not significant in this profile.

Sufficient oxygen supply is required to maintain the oxic front in the middle profile. Downward transferring alone cannot result in oxic front, because oxygen may be consumed in the reducing environment of the upper profile, and horizontal transfer of extra oxygen is thus expected. It is worth noting that the oxic front coincides with high water content in the middle profile. As shown in Fig. 3, LOI, which mainly represents the positive water in minerals of the weathering products, exhibits peak values of about 18% at 3.0 m. Also, gibbsite contents are high in this section (Fig. 3). Such high water content suggests the influence of groundwater. Therefore, the oxygen required by the oxic environment in the middle profile is most likely transported by groundwater. However, in-situ measurement of the water table has not been carried out in this area, and fluctuation of the water table in this region may be large because seasonal precipitation difference is significant. Further investigation is needed to decipher the exact mechanisms yielding the oxic environment in the middle profile.

Changes of redox conditions may also influence the distribution of Cr, in addition to Mn, Co and Ce. Cr is considered to be immobile during incipient chemical weathering (Middelburg et al., 1988; Nesbitt and Wilson, 1992). Significant loss of Cr is observed in the upper 3.0 m of this profile with percentage changes of Cr/Th ratios relative to the fresh basalt up to −50% in the top 2.0 m (Fig. 4a). Similar to Mn, loss of Cr decreases downwards in the profile, and Cr is even enriched in some parts below 3.0 m relative to the fresh basalt (Fig. 4a). Loss in the upper profile and enrichment in the lower profile for Cr may be related to organic matter, because organic colloids can improve the mobilization of Cr in aqueous solution, as in the case of Al (Dupre et al., 1999). However, the behavior of Cr during the change in redox condition is inverse to that of Mn (Middelburg et al., 1988; Marsh, 1991). Generally, Cr(III) is insoluble in reduced environments, whereas Cr(IV) is soluble in oxic environments (Middelburg et al., 1988; Marsh, 1991). This is clearly illustrated in Fig. 4a, where high values of percentage change of Cr/Th ratio generally correspond to low values for Mn/Th ratio, in the section below 3.0 m. Moreover, Cr concentrations show significant negative correlation with those of Mn and Co. In the lower profile, the negative correlations are very robust, with coefficients of −0.84 and −0.91 for Mn and Co, respectively (Fig. 4b and c). Moderate negative correlation can also be seen in the upper profile. This indicates different behaviors

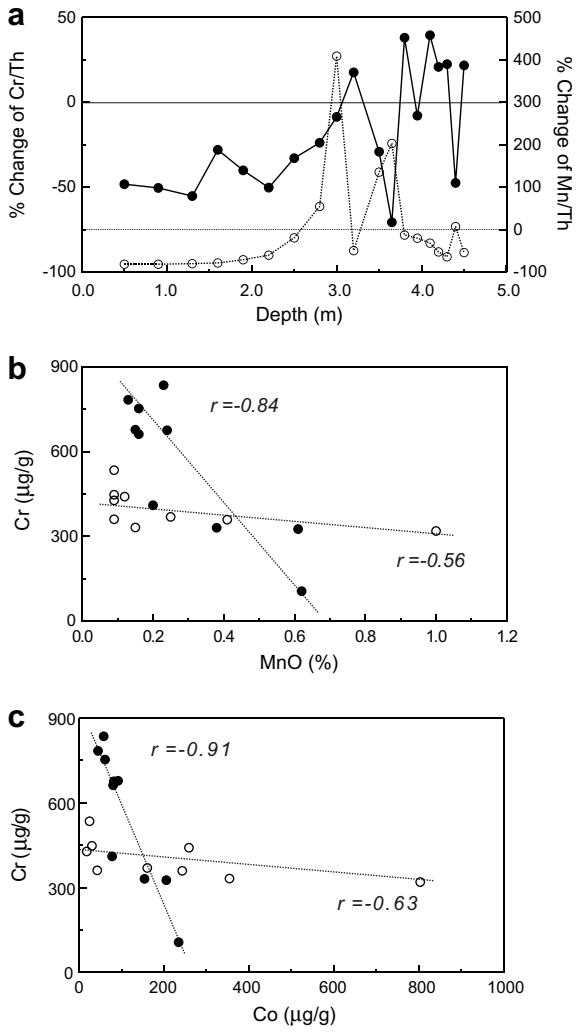

Fig. 4. Comparison between Cr, Co and Mn in the profile. (a) Variations of the percentage changes of Cr/Th ratios (solid line) and Mn/Th ratios (dashed line); (b) correlation between Cr and Mn concentrations; (c) correlation between Cr and Co concentrations. Open circles in (b) and (c) indicate samples in the upper 3 m, and the solid circles indicate those below 3 m.

for Mn and Cr in response to changes of the redox condition in the profile.

5.3. Rare earth elements (REEs)

5.3.1. Re-distribution of REEs

In general, REEs are released from primary minerals during chemical weathering, and are retained in weathering products (Nesbitt, 1979; Duddy, 1980; Price et al., 1991; Mongelli, 1993; Boulange and Colin, 1994). During extensive weathering, however, REEs are also removed from weathering products, with LREEs being less mobile than HREEs (Nesbitt, 1979). It is worth noting that the behavior of Ce is different from other REEs, because it is sensitive to changes of redox condition (Braun et al., 1990). Mobilization and re-distribution of Ce in this profile have been discussed above. Fig. 5 shows the in-depth variations for the percentage changes of REEs, excluding Ce to Th ratios, relative to fresh basalt. All these REEs show similar variation patterns. They are significantly removed from the upper profile (above 3.0 m) and are enriched in the lower profile with maximum enrichment occurring in 3.5 m, which is about 0.5 m below the section of maximum Ce enrichment (Fig. 5). In the Ce-enriched layer (3.0 m), significant enrichment of Gd is also observed, but enrichment of other REEs is not obvious. Estimated from percentage changes of REEs/Th ratios relative to fresh basalt, loss in the upper profile is about 30%, 50%, 60% and 70% for La, Pr, Nd and Sm, respectively. Losses of HREEs (from Eu to Lu) are very similar, about 80%. Conversely, LREE enrichment is much higher than that of HREE in the lower profile. The maximum percentage changes of LREE/Th ratios relative to the fresh basalt are about 300–350, but about 200–250 for HREE/Th ratios (Fig. 5). This indicates that losses of LREEs are less than those of HREEs in the upper profile, but enrichments in the lower profile are even larger, which agrees with the relative mobility of REEs during chemical weathering. LREEs are less mobile than HREEs, and the behavior for individual HREEs (Eu to Lu, except for Gd) is very similar to each other during extreme weathering.

Again, acid environment and organic matter may account for the removal and distribution of REEs in the profile. Similar to Al and Th, the transport of REEs can be significantly enhanced by complexing with organic colloids (Dupre et al., 1999; Oliva et al., 1999). Mobilized in the acid upper profile, the REEs are transferred downwards with organic matter by aqueous solution. When they reach the middle profile, at about 3.5 m, the organic matter is largely decomposed, and the capacity for carrying REEs dramatically decreases, resulting in significant REE precipitation in this section (Fig. 5). There is another REE enrichment in the lower section below 4.2 m. Unlike those in the middle profile, TOC concentrations in the lower profile are high (Fig. 5). Why these REEs have not been carried away by organic matter is not yet well understood. Different hosts for the REEs in the middle and the lower profiles may partially account for this. This will be discussed in following. Fe oxides/hydroxides, a potential phase to concentrate REEs (Pokrovsky et al., 2006), seems to not contribute much to these REE enrichments, because the percentage changes of Fe/Th ratios relative to the fresh basalt are close to zero in the sections enriched in REE (Fig. 5).

Several mineral groups have been suggested as the main host of REEs in weathering products. Clay minerals, such as vermiculite, are believed to be important hosts of both LREE and HREE (Duddy, 1980; Condie, 1991). Secondary phosphate minerals, such as apatite, which are transformed from important REE-bearing minerals, can concentrate REEs in weathering products, with the exception of Ce (Banfield and Eggleton, 1989; Braun et al., 1993). Some other studies suggest that enrichment of REEs is related to Mn oxides/hydroxides (Rankin and Childs, 1976; Koppi et al., 1996), and Fe oxides/hydroxides (Pokrovsky et al., 2006). Fig. 6 shows the correlation between concentrations of REEs (excluding Ce) and P, Fe, Mn and Al in this profile. Moderate negative correlation occurs between Al and

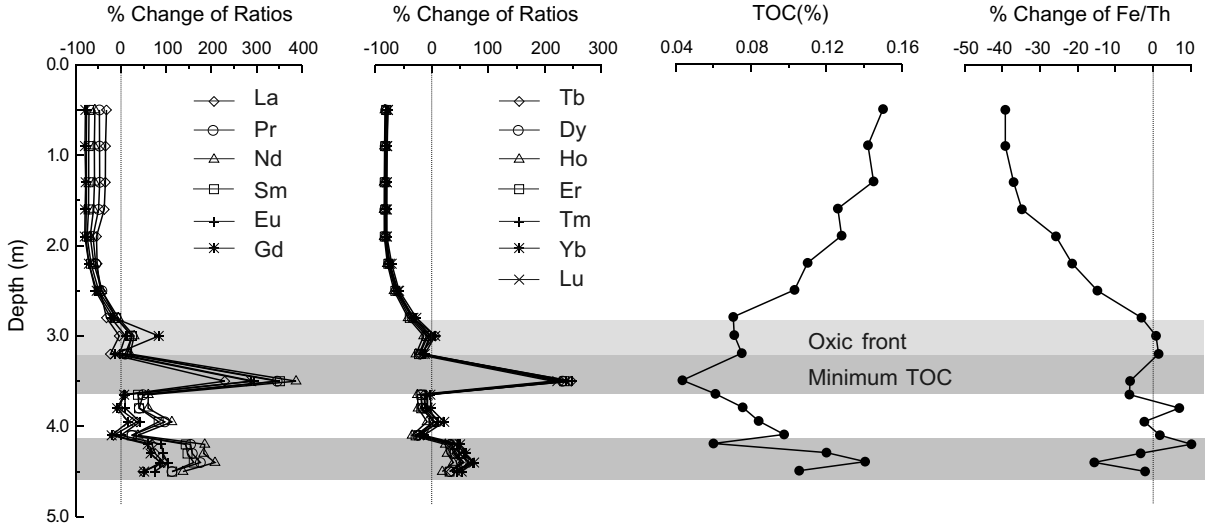

Fig. 5. Variations of the percentage changes of REEs (except Ce) to Th ratios relative to the fresh basalt in the profile. Variation of TOC and percentage change of Fe/Th ratios relative to the fresh basalt are also shown for comparison. The shaded bars indicate the oxic front and the REE enrichment sections. Gd enrichment, about 83%, is observed in the oxic front.

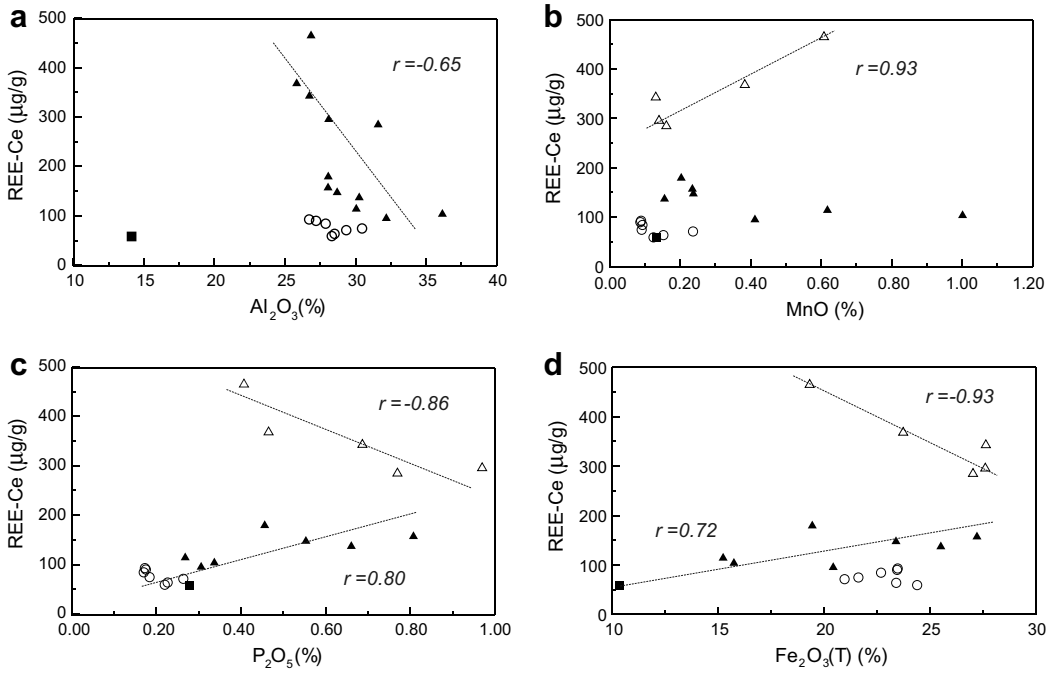

Fig. 6. Correlations between total REE concentrations (Ce excluding) and Al, Mn, P and Fe. (a) REE-Al_2O_3; (b) REE-MnO; (c) REE-P_2O_5; (d) REE-Fe_2O_3(T). Solid squares indicate the fresh basalt; open circles indicate samples in the upper 2.5 m; triangles (both open and solid) indicate the samples below 2.5 m, and open triangles in (b), (c) and (d) indicate samples with total REEs (Ce excluded) higher than 250 μg/g, which includes the maximum enrichment sample at 3.5 m and the samples below 4.2 m.

total REEs (excluding Ce) (Fig. 6a), indicating that clay minerals are not important hosts for REEs in this profile. Positive correlations are observed between total REEs (excluding Ce) and P, Fe and Mn. However, these correlations vary with REE concentrations. At high concentrations (>250 μg/g), REEs (excluding Ce) are positively correlated with Mn, with a coefficient of about 0.93 (Fig. 6b), but negatively correlated with P and Fe, with a coefficient of about −0.86 and −0.93, respectively (Fig. 6c and d). At low concentrations (<250 μg/g), significant positive correlations are observed between REEs and P and Fe, with a coefficient of about 0.80 and 0.72, respectively, but correlation with Mn is poor. This suggests that Mn oxides/hydroxides, as well as secondary phosphate minerals and Fe oxides/hydroxides are possible hosts of REE in this profile. It is worth noting that the five high REE samples include the maximum enrichment at 3.5 m and enrichments below 4.2 m. The later is accompanied by relatively high TOC contents. The positive correlation between REE and Mn concentrations below 4.2 m suggests that REEs in this section are associated with Mn oxides/hydroxides other than Fe oxides/hydroxides and secondary phosphate minerals, and they seem more resistant to transfer by organic matter. However, it is currently not well known how organic matters combine with REEs, and how REEs stay in the hosts. A detailed mineralogical characterization of REE-bearing phases would be necessary to answer this question.

5.3.2. Fractionation of REEs

Mobility differences of REEs during weathering may result in REE fractionation in weathering profiles. In general, the lower mobility of LREEs compared to HREEs may result in significant HREE depleted patterns in weathering products after extensive weathering, and mobility differences between Ce and other REEs usually results in Ce anomalies in weathering products (Nesbitt, 1979; Duddy, 1980; Banfield and Eggleton, 1989; Braun et al., 1990, 1993; Marsh, 1991; Price et al., 1991; Mongelli, 1993; Condie et al., 1995; Nesbitt and Markovics, 1997; Aubert et al., 2001; Patino et al., 2003). REE patterns normalized to the fresh basalt in this profile are shown in Fig. 8. In the upper profile (above 2.5 m), the weathering products exhibit HREE depleted patterns, and the maximum depletion relative to the fresh basalt occurs for Dy, Ho and Er (Fig. 7a). In the lower profile (below 2.5 m), all REEs are enriched compared to the fresh basalt, and the patterns are similar to those in the upper profile, with more enrichment for LREE than for HREE (Fig. 7b). However, La is generally depleted compared to Pr, Nd and Sm (Fig. 7a and b). Such patterns agree with the differences in mobility of REEs during extreme weathering.

Several strong Ce anomalies are identified in this profile. The ratio Ce/Ce*, defined as $Ce/Ce^* = 2Ce_n/(La_n + Pr_n)$, where the subscription n indicates normalization by the fresh basalt, was adopted to describe Ce anomalies of the weathering products. Only two of the samples exhibited significant negative Ce anomalies, with Ce/Ce* of 0.68 and 0.47 for samples HK06-12 and HK06-17, respectively. Ce concentration in HK06-12 is about 5 times higher than that in the fresh basalt. La and Pr concentrations, however, are greater by about a factor of 7–9. A similar situation occurs for sample HK06-17. In contrast, many other samples exhibit significant positive Ce anomalies, with maximum Ce/Ce* up to 20. Large positive Ce anomalies are usually

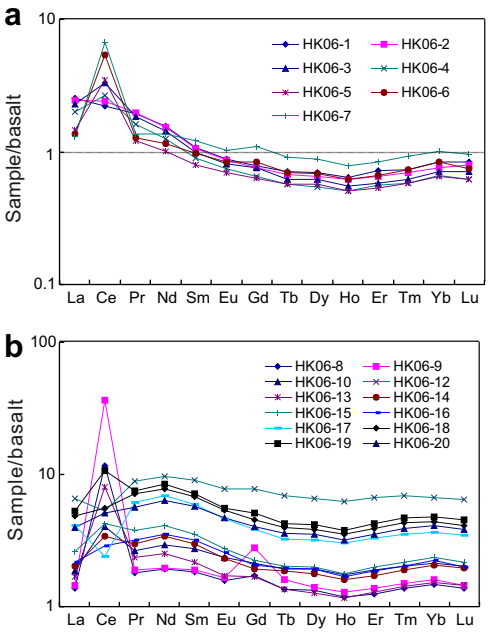

Fig. 7. REE patterns normalized to the fresh basalt. (a) Samples above 2.5 m; (b) samples below 2.5 m.

accompanied with high Ce concentrations, and generally occur in the middle of the profile (samples HK06-5 to HK06-13). This results from preferential precipitation of Ce as cerianite in oxic environments compared to La and Pr (Braun et al., 1990).

Significant positive Gd anomalies, $Gd/Gd^* = 3Gd_n/(Sm_n + 2Tb_n)$, are also observed in this profile (Fig. 8). The positive Gd anomalies mainly occur in the middle profile, 2.0–3.0 m, with a maximum value ~1.63 occurring at 3.0 m, corresponding to the maximum positive Ce anomalies. Correlation between the Ce anomalies and Gd anomalies is excellent, with a correlation coefficient up to 0.97 (Fig. 8). A positive Gd anomaly has been shown in some other profiles or weathering products (Rankin and Childs, 1976; Braun et al., 1990; Marsh, 1991; Koppi et al., 1996). Very little is known about the origin of the Gd anomaly. Braun et al. (1993) considered it to be the result of analytical artifacts due to isobaric interference of CeO on Gd during ICP-MS measurement. However, the positive Gd anomalies in our profile are not analytical artifacts. $^{142}Ce^{16}O$ isobaric interference may occur during ICP-MS measurement on ^{158}Gd when Ce concentration is very high. However, Gd was measured on ^{157}Gd for our samples. Potential isobaric interference on ^{157}Gd may originate from $^{141}Pr^{16}O$. However, as concentrations of Pr in our samples are similar to Gd (Table 1), and the oxide productivity is generally less than 2% on our ICP-MS, isobaric interference of $^{141}Pr^{16}O$ on ^{157}Gd is within the range of analytic errors, i.e., about 5%. Therefore, it can be concluded that Gd anomalies of these samples are real geological records.

Changes in redox conditions cannot contribute to the Gd anomaly, because Gd has no variable valence. Preferential scavenging of Gd by cerianite cannot account for such Gd anomalies either, because cation radii for Sm^{3+}, Eu^{3+}, Gd^{3+} and Tb^{3+} are all similar to that for Ce^{4+}. If scavenging happens, they will all be adsorbed or combined into cerianite together, resulting in no Gd anomalies. One possible explanation is variable REE-organic stability constants. As mentioned above, organic matters play a very important role in REE transport and enrichment in this profile. Stability constants of Gd complexes with organic ligands are generally smaller than those for Eu, and Tb (Lee and Byrne, 1993); thus, the capacity for organic materials to carry Gd is less than its neighbor REEs (Lee and Byrne, 1993). Consequently, during the downward transfer of the REEs in association with organic ligands, organic matter is successively oxidized and decomposed. Gd is preferentially released and precipitates elsewhere, producing positive Gd anomalies in the weathering products. At the oxic front in the middle profile, enhanced OM decomposition induces preferential precipitation of Gd relative to its neighbor REEs, and occurs with maximum Ce precipitation. As a result, both Gd and Ce anomalies show maximum positive values in this section.

6. SUMMARY

Elemental geochemistry of weathering profiles developed on Neogene basalts in northern Hainan Island, South China, enables us to investigate mobilization and re-distri-

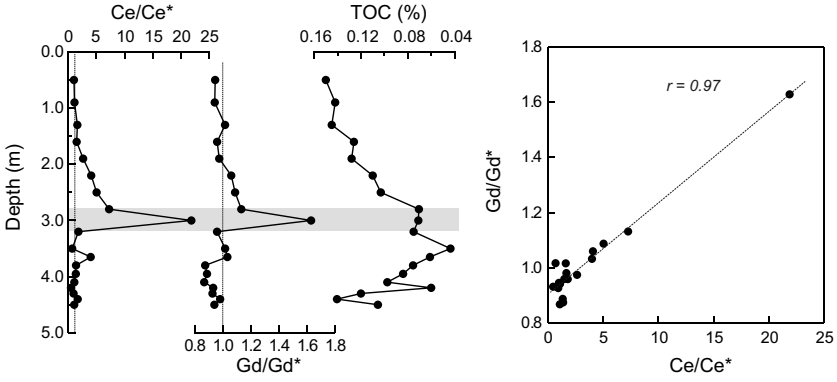

Fig. 8. In-depth variations of Ce anomalies, Gd anomalies and TOC concentrations, and correlation between Ce and Gd anomalies. The shaded bar indicates the oxic front, where maximum Ce and Gd positive anomalies occur.

bution of major and trace elements during advanced to extreme weathering of basalt. Details of the mobilization and re-distribution of elements are as follows:

(1) Among Fe, Ti, Zr, Hf, Nb and Ta, as Th, the general conservative elements during chemical weathering, Th is the most immobile during extreme chemical weathering in this profile. The percentage changes of the other elements to Th ratios relative to the fresh basalt suggest that Fe, Ti, Zr, Hf, Nb and Ta are significantly (about 20–40%) removed in the top 1 m of the profile. The losses of these elements decrease gradually downward in the profile. In the lower profile (below 3 m), Fe, Ti and Ta are as conserved as Th with percentage changes of their ratios to Th within the range ±5% relative to the fresh basalts. Slight losses of Zr and Nb are expected for the percentage of Zr/Th and Nb/Th of about −12% and −6%, respectively, whereas about 8% is expected for Hf/Th, suggesting a slight gain of Hf in the lower profile.
(2) Mobilization of Al, Mn, Co, Ce and U in the upper profile vary considerably, up to 80% of Mn, 95% of Co and 50% of Al being removed, but no U is removed. All these elements are remarkably enriched in the middle profile (2.5–3.7 m), with maximum enrichment up to 23 times that of the fresh basalt for Ce, 4 times for Mn and Co, and 120% and 70% higher for U and Al, respectively, at 3.0 m. These enrichments are accompanied by significant decreases of TOC concentration and the absence of organic nitrogen, as well as higher water contents in the middle profile, but no significant Fe precipitation. This suggests that organic matter plays an important role in transferring these elements, and the contribution of Fe-colloids is less important in this profile. Changes of redox condition, coupled with changes of organic matter content, account for the enrichment of Al, Mn, Ce in the middle profile and U enrichment, which is associated with precipitation of cerianite. Changes of redox condition also influence the distribution of Cr, which shows significant negative correlation with Mn.
(3) REEs, except Ce, are removed during extreme weathering, and the removal of HREE (about 68–80%) is more than LREE, about 30–40% for La and Pr. However, they are all remarkably enriched in the middle and the lower profile. The transport and enrichment of REEs are also closely associated with organic matter. Mn oxides/hydroxides, as well as secondary phosphate minerals and Fe oxides/hydroxides are all possible hosts for REEs, and significant REE enrichment below 4.2 m seems to be mostly associated with Mn oxides/hydroxides. Clay minerals, however, are not important host for REEs in this profile.
(4) Both Ce anomalies and Gd anomalies are obvious in the weathering products, and Gd anomalies are closely related to Ce anomalies. Differences in the stabilities of complexes formed by REEs with organic ligands are likely to account for Gd anomalies. Successive decomposition of organic matter results in positive Gd anomalies in the profile, and this is closely related to a change of redox condition, which results in Ce anomalies.

ACKNOWLEDGMENTS

We are most grateful to Ying Liu, Xiangling Tu, Huizhi Zhang of Guangzhou Institute of Geochemistry, CAS for their assistance on XRF, ICP-MS and organic element analysis, respectively. The authors thank J. Schott, J.J. Braun, and another two anonymous reviewers for their critical comments and constructive suggestions, which helped to improve the manuscript. This study was supported by the Chinese Academy of Sciences (Grant KZCX3-SW-152-2), the National Natural Science Foundation of China (Grant 40473012) and the Guangzhou Institute of Geochemistry, CAS (Grant GIGCX-04-05).

REFERENCES

Aubert D., Stille P., and Probst A. (2001) REE fractionation during granite weathering and removal by waters and suspended loads: Sr and Nd isotopic evidence. *Geochim. Cosmochim. Acta* **65**(3), 387–406.

Banfield J. F., and Eggleton R. A. (1989) Apatite replacement and rare earth mobilization, fractionation, and fixation during weathering. *Clay Clay Miner.* **37**(2), 113–127.

Berner R. A., Berner E. K. (1997) Silicate weathering and climate. In *Tectonic uplift and climate change* (ed. W. F. Ruddiman). Plenum Press, pp. 353–365.

Boulange B., and Colin F. (1994) Rare-earth element mobility during conversion of nepheline syenite into lateritic bauxite at Passa-Quatro, Minais-Gerais, Brazil. *Appl. Geochem.* **9**(6), 701–711.

Braun J. J., Ngoupayou J. R. N., Viers J., Dupre B., Bedimo J. P. B., Boeglin J. L., Robain H., Nyeck B., Freydier R., Nkamdjou L. S., Rouiller J., and Muller J. P. (2005) Present weathering rates in a humid tropical watershed: Nsimi, South Cameroon. *Geochim. Cosmochim. Acta* **69**(2), 357–387.

Braun J. J., Pagel M., Herbillon A., and Rosin C. (1993) Mobilization and redistribution of Rees and Thorium in a syenitic lateritic profile—a mass-balance study. *Geochim. Cosmochim. Acta* **57**(18), 4419–4434.

Braun J. J., Pagel M., Muller J. P., Michard A., and Guillet B. (1990) Cerium anomalies in lateritic profiles. *Geochim. Cosmochim. Acta* **54**, 781–795.

Braun J. J., Viers J., Dupre B., Polve M., Ndam J., and Muller J. P. (1998) Solid/liquid REE fractionation in the lateritic system of Goyoum, east Cameroon: the implication for the present dynamics of the soil covers of the humid tropical regions. *Geochim. Cosmochim. Acta* **62**(2), 273–299.

Brimhall G. H., Lewis C. J., Ford C., Bratt J., Taylor G., and Warin O. (1991) Quantitative geochemical approach to pedogenesis—importance of parent material reduction, volumetric expansion, and eolian influx in lateritization. *Geoderma* **51**(1–4), 51–91.

Caggianelli A., Fiore S., Mongelli G., and Salvemini A. (1992) Ree distribution in the clay fraction of pelites from the southern Apennines, Italy. *Chem. Geol.* **99**(4), 253–263.

Chesworth W., Dejou J., and Larroque P. (1981) The weathering of basalt and relative mobilities of the major elements at Belbex, France. *Geochim. Cosmochim. Acta* **45**, 1235–1243.

Condie K. C. (1991) Another look at rare-earth elements in shales. *Geochim. Cosmochim. Acta* **55**(9), 2527–2531.

Condie K. C., Dengate J., and Cullers R. L. (1995) Behavior of rare-earth elements in a paleoweathering profile on granodiorite in the front range, Colorado, USA. *Geochim. Cosmochim. Acta* **59**(2), 279–294.

Cornu S., Lucas Y., Lebon E., Ambrosi J. P., Luizao F., Rouiller J., Bonnay M., and Neal C. (1999) Evidence of titanium mobility in soil profiles, Manaus, central Amazonia. *Geoderma* **91**(3–4), 281–295.

Craig D. C., and Loughnan F. C. (1964) Chemical and mineralogical transformations accompanying the weathering of basic volcanic rocks of Nes South Wales: Australian. *J. Soil Sci.* **2**, 218–234.

Dequincey O., Chabaux F., Clauer N., Sigmarsson O., Liewig N., and Leprun J. C. (2002) Chemical mobilizations in laterites: evidence from trace elements and U-238–U-234–Th-230 disequilibria. *Geochim. Cosmochim. Acta* **66**(7), 1197–1210.

Duddy L. R. (1980) Redistribution and fractionation of rare-earth and other elements in a weathering profile. *Chem. Geol.* **30**, 363–381.

Dupre B., Viers J., Dandurand J. L., Polve M., Benezeth P., Vervier P., and Braun J. J. (1999) Major and trace elements associated with colloids in organic-rich river waters: ultrafiltration of natural and spiked solutions. *Chem. Geol.* **160**(1–2), 63–80.

Froelich P. N., Klinkhammer G. P., Bender M. L., Luedtke N. A., Heath G. R., Cullen D., Dauphin P., Hammond D., Hartman B., and Maynard V. (1979) Early oxidation of organic-matter in pelagic sediments of the eastern equatorial atlantic—suboxic diagenesis. *Geochim. Cosmochim. Acta* **43**(7), 1075–1090.

Harnois L. (1988) The CIW index: a new chemical index of weathering. *Sediment. Geol.* **55**, 319–322.

Harriss R. C., and Adams J. A. S. (1966) Geochemical and minerological studies on the weathering of granitic rocks. *Am. J. Sci.* **264**, 146–173.

Hill I. G., Worden R. H., and Meighan I. G. (2000) Yttrium: the immobility-mobility transition during basaltic weathering. *Geology* **28**(10), 923–926.

Huang Z. G., Cai F. X., Han Z. Y., Chen J. H., Zong Y. Q., and Lin X. D. (1993) *Quaternary Volcano in Leizhou Peninsula and Hainan Island*. Science Press.

Koppi A. J., Edis R., Field D. J., Geering H. R., Klessa D. A., and Cockayne D. J. H. (1996) Rare earth element trends and cerium–uranium–manganese associations in weathered rock from Koongarra, northern territory, Australia. *Geochim. Cosmochim. Acta* **60**(10), 1695–1707.

Kurtz A. C., Derry L. A., Chadwick O. A., and Alfano M. J. (2000) Refractory element mobility in volcanic soils. *Geology* **28**(8), 683–686.

Lee J. H., and Byrne R. H. (1993) Complexation of trivalent rare-earth elements (Ce, Eu, Gd, Tb, Yb) by carbonate ions. *Geochim. Cosmochim. Acta* **57**(2), 295–302.

Li X. H., Liu Y., Tu X. L., Hu G. Q., and Zeng W. (2002) Precise determination of chemical compositions in silicate rocks using ICP-AES and ICP-MS. A comparative study of sample digestion techniques of alkali fusion and acid dissolution (in Chinese with English abstract). *Geochimica* **31**(3), 289–294.

Liu Y., Liu H. C., and Li X. H. (1996) Simultaneous and precise determination of 40 trace elements in rock samples using ICP-MS (in Chinese with English abstract). *Geochimica* **25**(6), 552–558.

Marsh J. S. (1991) Ree fractionation and Ce anomalies in weathered karoo dolerite. *Chem. Geol.* **90**(3–4), 189–194.

Melfi A. J., Subies F., Nahon D., and Formoso M. L. L. (1996) Zirconium mobility in bauxites of southern Brazil. *J. S. Am. Earth Sci.* **9**(3–4), 161–170.

Middelburg J. J., Van der Weijden C. H., and Woittiez J. R. W. (1988) Chemical processes affecting the mobility of major, minor and trace elements during weathering of granitic rocks. *Chem. Geol.* **68**, 253–273.

Mongelli G. (1993) Ree and other trace-elements in a granitic weathering profile from Serre, Southern Italy. *Chem. Geol.* **103**(1–4), 17–25.

Mongelli G. (1997) Ce-anomalies in the textural components of upper Cretaceous karst bauxites from the Apulian carbonate platform (southern Italy). *Chem. Geol.* **140**(1–2), 69–79.

Nahon D. (2003) Weathering in tropical zone. Significance through ancient and still active mechanisms. *C. R. Geoscience* **335**(16), 1109–1119.

Nahon D., and Merino E. (1996) Pseudomorphic replacement versus dilation in laterites: petrographic evidence, mechanisms, and consequences for modelling. *J. Geochem. Explor.* **57**(1–3), 217–225.

Nesbitt H. W. (1979) Mobility and fractionation of rare earth elements during weathering of granodiorite. *Nature* **279**, 206–210.

Nesbitt H. W., and Markovics G. (1997) Weathering of granodioritic crust, long-term storage of elements in weathering profiles, and petrogenesis of siliciclastic sediments. *Geochim. Cosmochim. Acta* **61**(8), 1653–1670.

Nesbitt H. W., Markovics G., and Price R. C. (1980) Chemical processes affecting alkalis and alkaline earths during continental weathering. *Geochim. Cosmochim. Acta* **44**, 1659–1666.

Nesbitt H. W., and Wilson R. E. (1992) Recent chemical-weathering of basalts. *Am. J. Sci.* **292**(10), 740–777.

Nesbitt H. W., Young G. M., McLennan S. M., and Keays R. R. (1996) Effects of chemical weathering and sorting on the petrogenesis of siliciclastic sediments, with implications for provenance studies. *J. Geol.* **104**(5), 525–542.

Oliva P., Viers J., Dupre B., Fortune J. P., Martin F., Braun J. J., Nahon D., and Robain H. (1999) The effect of organic matter on chemical weathering: study of a small tropical watershed: Nsimi-Zoetele site, Cameroon. *Geochim. Cosmochim. Acta* **63**(23–24), 4013–4035.

Parker A. (1970) An index of weathering for silicate rocks. *Geol. Mag.* **107**, 501–504.

Patino L. C., Velbel M. A., Price J. R., and Wade J. A. (2003) Trace element mobility during spheroidal weathering of basalts and andesites in Hawaii and Guatemala. *Chem. Geol.* **202**(3–4), 343–364.

Patino L. C., Velbel M. A., Price J. R., and Wade J. A. (2005) Element redistribution during weathering of volcanic rocks in sedentary landscapes. *Geochim. Cosmochim. Acta* **69**(10), A683.

Pokrovsky O. S., Schott J., and Dupre B. (2006) Trace element fractionation and transport in boreal rivers and soil porewaters of permafrost-dominated basaltic terrain in Central Siberia. *Geochim. Cosmochim. Acta* **70**(13), 3239–3260.

Price R. C., Gray C. M., Wilson R. E., Frey F. A., and Taylor S. R. (1991) The effects of weathering on rare-earth element, Y and Ba abundances in tertiary basalts from southeastern Australia. *Chem. Geol.* **93**(3–4), 245–265.

Rankin P. C., and Childs C. W. (1976) Rare-earth elements in iron–manganese concretions from some New Zealand soils. *Chem. Geol.* **18**, 55–64.

Viers J., Dupre B., Braun J. J., Deberdt S., Angeletti B., Ngoupayou J. N., and Michard A. (2000) Major and trace element abundances, and strontium isotopes in the Nyong basin rivers (Cameroon): constraints on chemical weathering processes and elements transport mechanisms in humid tropical environments. *Chem. Geol.* **169**(1–2), 211–241.

Viers J., Dupre B., Polve M., Schott J., Dandurand J. L., and Braun J. J. (1997) Chemical weathering in the drainage basin of

a tropical watershed (Nsimi-Zoetele site, Cameroon): comparison between organic-poor and organic-rich waters. *Chem. Geol.* **140**(3–4), 181–206.

Wei G. J., Liu Y., Li X. H., Shao L., and Fang D. Y. (2004) Major and trace element variations of the sediments at ODP Site 1144, South China Sea, during the last 230 ka and their paleoclimate implications. *Palaeogeogr. Palaeocl.* **212**(3–4), 331–342.

Windom H. L. (1976) Lithogeneous materials in marine sediments. In *Chemical Oceanograpgy*, vol. 5 (eds. J. P. Riley and R. Chester). Academic Press, pp. 103–135.

Young G. M., and Nesbitt H. W. (1998) Processes controlling the distribution of Ti and Al in weathering profiles, siliciclastic sediments and sedimentary rocks. *J. Sediment. Res.* **68**(3), 448–455.

Zabel M., Schneider R. R., Wagner T., Adegbie A. T., de Vries U., and Kolonic S. (2001) Late Quaternary climate changes in central Africa as inferred from terrigenous input to the Niger fan. *Quatern. Res.* **56**(2), 207–217.

Zhu B. Q., and Wang H. F. (1989) Nd–Sr–Pb isotopic and chemical evidence for the volcanism with MORB-OIB source characteristics in the Leiqiong Area, China. *Geochimica* **18**(3), 193–201.

Associate editor: Jacques Schott